

LONGITUDINAL STABILITY PARAMETERS FOR FLYING BOOM AERIAL REFUELING

Luke H. Peristy¹ & Ruben E. Perez²

¹Doctoral Candidate, Department of Mechanical and Aerospace Engineering, Royal Military College of Canada Kingston, ON, K7K 7B4, Canada

Abstract

This paper uses a combination of computational methods to analyze the flight mechanics and dynamics of two large transport aircraft, the C-17 and C-5, during flying boom air-to-air refueling. These two aircraft were considered due to their similarity in geometry, but radically different performances during air-to-air procedures. The paper introduces a quantity related to positional stability called the positional static margin, which is then related to pilot responses to perturbations during the air-to-air procedure. The frequency and phase response of the aircraft and pilot is also examined, showing that the flight path control of the C-17 necessitates larger and higher frequency inputs than those of the C-5. A quantity called the time delay margin is also introduced, and it, together with the magnitude of the pilot response, is demonstrated to correlate with the experimentally observed increased risk of pilot-induced oscillations in the C-17 during air-to-air refueling.

Keywords: Air-to-Air Refueling, Flying Boom Refueling, Pilot Induced Oscillations

Nomenclature

α	=	Angle of attack (rad)
eta_{PG}	=	Prandtl-Glauert correction factor
Δz	=	Vertical separation between tanker and receiver (m)
δ	=	Elevator deflection (rad)
Γ	=	Vortex ring strength
γ	=	Flight path angle (rad)
ρ	=	Density of air (kg/m ³)
au	=	Tustin model time delay (s)
$a_{\Box\Box}$	=	Aerodynamic influence coefficient
AIC	=	Aerodynamic influence coefficient matrix
b	=	Wingspan (m)
\bar{c}	=	Mean aerodynamic chord (m)
c_p	=	Stick position (cm)
$(C_L, C_D, \text{ and } C_Y)$	=	Coefficient of lift, drag, and sideforce
$C_{L,lpha}$	=	Derivative of C_L with respect to α (rad ^{-1<})
$(C_l, C_m, \text{ and } C_n)$	=	Coefficient of roll, pitch, and yaw
$C_{m,lpha}$	=	Derivative of C_m with respect to α (rad ^{-1<})
D	=	Drag force (N)
e(s)	=	Error signal in the s-domain
f_c	=	Crossover frequency (rad/s)
I_{y}	=	Moment of Inertia about y (kg·m ²)

²Professor, Department of Mechanical and Aerospace Engineering, Royal Military College of Canada Kingston, ON, K7K 7B4, Canada

Tustin model pilot gain K_p Lift force (N) LVertical acceleration due to change in angle of attack (m/s) L_{α} Mach number M_{∞} Non-dimensionalized derivative of pitching moment M_{α} with respect to angle of attack (s^{-2}) Non-dimensionalized derivative of pitching moment $M_{\dot{\alpha}}$ with respect to $\dot{\alpha}$ (s⁻¹) Non-dimensionalized derivative of pitching moment M_q with respect to pitch rate (s^{-1}) Non-dimensionalized derivative of pitching moment M_{δ} with respect to elevator deflection (s^{-2}) Pitching moment (N·m) m Mass (kg) mNormal vector nDynamic pressure = $\frac{1}{2}\rho V^2$ (Pa) ā Boundary condition right-hand-side vector RHSS Wing area (m²) = Positional Static Margin SM_P Tustin model anticipation parameter T_L Indicates tanker Pitch rate (rad/s) p Indicates receiver = x, y, and z components of velocity (m/s) (u, v, w)= Freestream velocity vector (m/s) U_{∞} Wake velocity vector (m/s) U_{wake} Weight (N) W Y Side force (N) Acceleration in the Z direction due to Z_{α} a change in angle of attack, (m·s⁻²) Acceleration in the Z direction due to Z_{δ} a change in elevator deflection, $(m \cdot s^{-2})$

1 Introduction

With current interest in increasing fuel efficiency of civil aviation activities in order to reduce carbon footprint, air-to-air refueling (AAR) is a promising means to achieve these ends. AAR is already used in military aviation to increase mission lengths, and allow aircraft to stay airborne for much longer than would otherwise be possible. In addition, it has been demonstrated that a long haul flight with AAR requires less fuel compared to an identical mission with a layover for ground refueling [1]. An aircraft which receives fuel via mid-flight AAR can have a reduced initial take-off weight compared to a baseline mission that includes a stop-over for fuel. This results in fuel burn improvements via the overall reduction in power required (and therefore fuel used) during take-off, and also eliminates the need to land and take-off again following the stop-over. Nangia has suggested that reductions in fuel usage for international flights when using AAR would be between 30% and 40%, with commensurate cost savings [2]. Additionally, removing the need for a fuel stop-over also reduces the number of ground-air-ground cycles, increases the time between maintenance events, and improves the overall lifespan of an aircraft. While the benefits of civil AAR are numerous, its introduction as a regular industry practice will face significant regulatory hurdles, with Spencer predicting the various likely relevant certification considerations will include the CS-25 control and stability requirements for general stability, static longitudinal stability, static directional and lateral stability, and dynamic stability [3].

Early computational work on aircraft stability during AAR was performed by Bloy *et al.* first using a horseshoe vortex [4, 5] and then a vortex lattice method [6] to model the tanker wake and receiver aircraft. In the earlier work, Bloy noted oscillatory dynamic modes in the lateral-directional [4] and

longitudinal [5] modes which in practice required pilot input to damp. In later work, Bloy examined the effect of both tanker geometry and receiver geometry on receiving stability, finding a receiver with an elevated horizontal stabilizer showed static stability with respect to vertical position but was dynamically unstable. Blake *et al.* performed work, also with a vortex panel method, to predict areas of positional stability i.e. the tendency of the receiver to return to its original position when disturbed [7, 8], and also performed wind-tunnel tests to validate the response [8]. However, the aircraft model used were tailless delta wings, which were less representative of aircraft geometries frequently used in AAR. Subsequent work by Dogan and Blake examined bow wave effects during AAR using a lifting-line based vortex effect modeling technique with various sources and sinks, finding that they were able to capture the effect of a large receiver on the pitching moment of the tanker [9]. Okolo, Blake, and Dogan also examined positional stability but with applications for formation flight rather than AAR [10].

The oscillatory behaviours shown in Bloy's analysis of large aircraft refueling have also been noted in various flight tests, particularly in the case of the flying boom refueling of the C-17. Iloputaife *et al.* strongly implicated a variety of causes for deficient handling qualities during AAR, including the small frequency separation between the short period and control system dynamics, tanker geometry leading exhaust impingement on the C-17 horizontal stabilizer, and bow wave effects leading to poor stability of the tanker [11]. In the longitudinal axis, this was alleviated in part by reducing changing the pitch control sensitivity, with further improvements to the flight control law being subsequently documented by Weltz *et al.* which minimized the tendencies towards pilot-induced oscillations (PIOs) during the AAR task [12]. The presence of PIOs during AAR is not limited to large aircraft only, as Mitchell and Klyde used the probe-and-droge (PDR) AAR task with the F-14 as a test bed to examine PIO characteristics [13]. Additionally, Yin *et al.* have used simulator-based analyses of an F-16 to suggest new control law requirements to prevent PIOs in pitch during flying-boom AAR [14].

In general, analysis of AAR represents a challenge at the intersection of aerodynamics, flight dynamics, control design, and human factors. Previous work by the authors utilized a similar methodology to the one presented in Section 2 for the purposes of examining the lateral-directional positional stability of a F-18 receiver during PDR. A major finding in that work was that the trim strategy used was a determining factor as to whether the receiver was positionally stable or unstable [15]. This work introduces new parameters which can be used to make predictions about aircraft stability during flying boom AAR, which could have implications for aircraft design, control system design, and later use in compatibility analysis for refueling large civil aircraft with different tanker platforms.

Section 2 of this abstract introduces a new positional stability quantity and the computational methodology used to examine its utility, and Section 3 presents the results of the analysis of two tanker-receiver pairs, namely a KC-135 tanker with a C-17 receiver and a KC-135 tanker with a C-5 receiver.

2 Methodology

The methodology uses a vortex panel method to predict the air velocities in the tanker wake and evaluate their effect on the receiver. This code has been used in other work by the authors for the purposes of evaluating positional stability and closed-loop dynamics of an F/A-18 receiver during probe-and-drogue refueling. [15]

2.1 Vortex Panel Method

A potential flow based vortex panel method was chosen to model the tanker and receiver aircraft, because it is a method that is easily adapted to different aircraft geometries, and has demonstrated the ability to capture the major features of a tanker's wake and the resultant forces and moments on a receiver at low computational cost. Despite the assumption of incompressibility, the vortex panel code used in this work uses a Prandtl-Glauert correction to extend the range of Mach numbers at which the code can produce valid results to $M_{\infty} = 0.7$, below which most AAR procedures take place. The vortex panel code is based on that of Katz and Plotkin [16]. The method models aircraft lifting surfaces with sets of closed panels made of vortex lines, hence vortex panel method. Each vortex

panel is associated with some vortex ring strengths (Γ), which are proportional to the lift generated by each panel. These vortex ring strengths are found using using a set of linear equations described by an aerodynamic influence coefficient (AIC) matrix, and boundary conditions given by the freestream velocity vector (U_{∞}), other external air velocities such as the wake of another aircraft, jetwash, or propwash (U_{wake}), and the set of normal vectors at surface collocation points (n). This will be elaborated on further using the schematic of a representative panel surface in Figure 1.

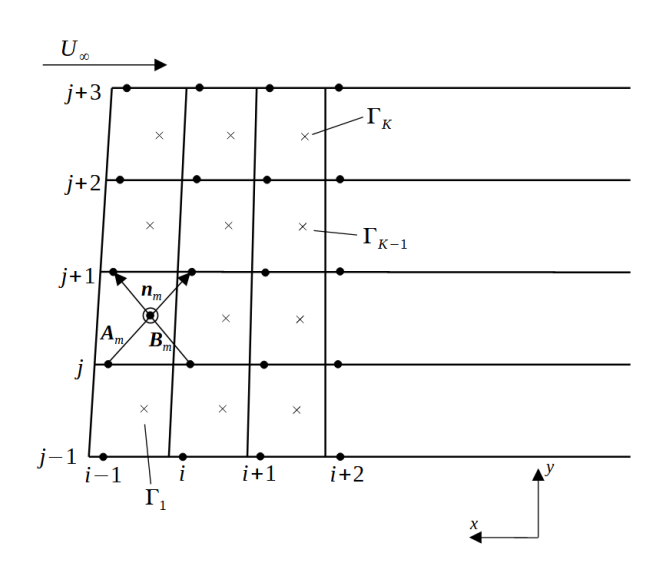


Figure 1 – Array of wing and wake panel corner points.

The above vortex panel surface has K panels in total. Each vortex panel is made up of vortex line elements whose vertices are defined by panel corner points (•) which are indexed in the x direction with the index i and indexed in the y direction with the index j. Each vortex panel is associated with some circulation strength Γ , a panel collocation point (\times) , and a normal vector n which is considered to originate at the collocation point. The direction of an example normal vector above, n_m , is defined by cross-product of two vectors, A_m and B_m , which themselves are defined by the panel corner points such that A_m extends from point (i-1,j) to point (i,j+1) and B_m extends from point (i,j) to (i-1,j+1). Figure 1 also shows vortex lines extending in the -x direction, which represent the prescribed flat wake of the vortex panel system extending from the trailing edges into the farfield.

The vortex panel circulation strengths, Γ , are found by ascribing the boundary condition that the net flow through each panel at its collocation point must be 0. This is done by calculating the aerodynamic influence coefficients (AIC) of each panel. The aerodynamic influence of panel l on the collocation point of panel m (a_{ml}) is given by the dot product

$$a_{ml} = (u_{\text{ind}}, v_{\text{ind}}, w_{\text{ind}})_{ml} \cdot n_m \tag{1}$$

where $(u_{\rm ind},v_{\rm ind},w_{\rm ind})_{ml}$ are the x,y, and z velocity components induced by vortex ring l at the collocation point of panel m. (Note that the coordinate systems used to define $(u_{\rm ind},v_{\rm ind},w_{\rm ind})_{ml}$ and n_m are not important as long as they are the same.) The influence of each ring vortex on each collocation point must be added. For a single collection of vortex panels, and assuming that the only external flow is the freestream velocity U_{∞} , at some collocation point m, the total influence from all K vortex rings must be such that

$$\sum_{l=1}^{K} a_{ml} \Gamma_l = -U_{\infty} \cdot n_m \tag{2}$$

which is to say that the velocity induced by every vortex panel at each collocation point must be equal and opposite to the freestream velocity component which is parallel to the panel's normal vector. A system of equations known as the AIC matrix is populated by influence coefficients of each vortex

ring at each collocation point using the above boundary condition. A full vortex panel system with K vortex rings and collocation points can be represented in matrix form as follows:

$$\begin{bmatrix} a_{11} & a_{12} & a_{13} & \dots & a_{1K} \\ a_{21} & a_{22} & a_{23} & \dots & a_{2K} \\ \vdots & \vdots & \vdots & \ddots & \vdots \\ a_{K1} & a_{K2} & a_{K3} & \dots & a_{KK} \end{bmatrix} \begin{pmatrix} \Gamma_1 \\ \Gamma_2 \\ \vdots \\ \Gamma_K \end{pmatrix} = \begin{pmatrix} -U_{\infty} \cdot n_1 \\ -U_{\infty} \cdot n_2 \\ \vdots \\ -U_{\infty} \cdot n_K \end{pmatrix}$$
(3)

By denoting the vector on the right hand side of the equation as RHS, Equation 3 can be represented as

$$AIC \Gamma = RHS \tag{4}$$

For a simple vortex lattice system, the circulation strengths Γ are found by inverting the AIC matrix. These Γ terms are then proportional to the lift generated by each panel, and the Γ corresponding to the wake vortex elements are proportional to the air velocities in the wake. By either adjusting the direction of the normal vectors of the tanker vortex panel system, or by changing the direction of the freestream vector in a way analogous to changing the aircraft's angle of attack, a solution of vortex ring strengths can be found such that the total lift generated is equal to the presumed weight of the aircraft which the vortex panel system is representing.

The force generated by each individual vortex panel on the leading edge of a surface is found via the following:

$$\Delta F_m = (\rho U_{\infty} \Gamma_m \Delta v_m) / \beta_{PG}^2$$
, for leading edge panels (5)

where Δy_m is the spanwise width of panel m. Additionally, a Prandtl-Glauert correction factor (β_{PG}) is applied when calculating lift, where $\beta_{PG} = \sqrt{1-M_{\infty}^2}$. The lift generated by non-leading edge panels is proportional to the difference in Γ between the panel and the panel directly in front of it. This is written mathematically as

$$\Delta F_m = \rho U_{\infty} (\Gamma_m - \Gamma_{m-(\text{number of spanwise panels})}) \Delta y_m / \beta_{PG}^2$$
, for all other panels (6)

The induced drag, normal force, and lift force are then found as the projection of ΔF_m into the x, y, and z directions respectively.

$$[\Delta D_m, \Delta Y_m, \Delta L_m] = \Delta F_m n \tag{7}$$

Once the vortex ring strengths for the tanker have been found, they can then be used to predict air velocities in the wake of the aircraft. For the case of a vortex panel system representing a receiver in the wake of a tanker, the wake velocities at each collocation point are then added to the freestream velocity vector in the RHS of the receiver vortex panel method equation as follows:

$$\begin{bmatrix} a_{11} & a_{12} & a_{13} & \dots & a_{1K} \\ a_{21} & a_{22} & a_{23} & \dots & a_{2K} \\ \vdots & \vdots & \vdots & \ddots & \vdots \\ a_{K1} & a_{K2} & a_{K3} & \dots & a_{KK} \end{bmatrix} \begin{Bmatrix} \Gamma_1 \\ \Gamma_2 \\ \vdots \\ \Gamma_K \end{Bmatrix} = \begin{Bmatrix} -(U_{\infty} + U_{\text{wake}}) \cdot n_1 \\ -(U_{\infty} + U_{\text{wake}}) \cdot n_2 \\ \vdots \\ -(U_{\infty} + U_{\text{wake}}) \cdot n_K \end{Bmatrix}$$
(8)

where the $U_{\rm wake}$ term consists of the air velocities in the tanker's wake. Simple jet effects from the tanker are included by assuming a streamtube of fixed radius emanating from the engines, inside which is a fixed jet velocity is added to the term $U_{\rm wake}$. Having found the lift generated by each vortex panel, we also define the vector r_j which is the vector from the aircraft's presumed centre of gravity (CG) to the collocation point of panel j. From this, the individual contribution of each panel to the aircraft's rolling moment l, pitching moment m, and yawing moment m can be calculated as follows:

$$[l,m,n]_j = (\Delta F_j n_j \times r_j) \tag{9}$$

The total moment being imposed on the aircraft can be found by summing the contribution of all panels.

$$[l,m,n] = \sum_{j=1}^{K} \Delta F_j n_j \times r_j \tag{10}$$

These moments can be converted into moment coefficients via the following set of normalizations:

$$C_l = \frac{l}{0.5\rho U_{\infty}^2 Sb} \tag{11}$$

$$C_m = \frac{m}{0.5\rho U_\infty^2 S\bar{c}} \tag{12}$$

$$C_n = \frac{n}{0.5\rho U_{\infty}^2 Sb} \tag{13}$$

The governing equations for the tanker are such that the tanker is in steady level flight, where its total lift is equal to its weight and the aircraft is trimmed in pitch.

$$L_t = W_t \qquad \text{and} \qquad m_t = 0 \tag{14}$$

For the receiver, we enforce that the aircraft is generating lift equal to its weight, and that it is in trimmed rolling moment, pitching moment, and yawing moment (n). However, for this case of flying boom refueling where the aircraft are flying with parallel centrelines, we assume there will be negligible external sources of rolling moment and yawing moment.

$$L_r = W_r \qquad \text{and} \qquad m_r = 0 \tag{15}$$

Fuselage effects are also neglected, as the displacement of air due to the physical volume of fuselage elements primarily manifests as a bow-wave from the receiver affecting the trim condition of the tanker. Dogan *et al.* estimated that the bow wave effect accounts for an increase of 3% of the total lift, which is roughly equal to the effect of the upwash from bound vortex on the receiver's main lifting surface. [17] The effect of the tanker's fuselage and other volume elements on the receiver is considered negligible for large receivers, although Jackson *et al.* have found that the downwash effect of the flying boom itself may be not be negligible when considering small receivers. [18]

2.2 Positional Static Margin

Bloy and Gingras discuss positional stability as an important aspect of close formation flight, such as is typical during the AAR task. Positional stability refers to the tendency of the receiver aircraft to return to its original position relative to the tanker when disturbed [8]. Using both wind tunnel and potential flow calculations, they investigated positional stability derivatives including $\frac{\partial C_L}{\partial z}$ and $\frac{\partial C_M}{\partial z}$. is the change in lift per change in vertical separation z, and $\frac{\partial C_M}{\partial z}$ is the change in pitching moment per change in vertical separation z. For typical stability axes, positional stability requires

$$\frac{\partial C_L}{\partial z} > 0$$
 and $\frac{\partial C_m}{\partial z} > 0$

i.e. to ensure positional stability, an increase in vertical separation between tanker and receiver should result in an increase in lift coefficient in the case of $\frac{\partial C_L}{\partial z}$, and a nose up pitching moment in the case of $\frac{\partial C_m}{\partial z}$. A receiver aircraft at trim is typically positionally stable in in the derivative $\frac{\partial C_L}{\partial z}$ when flying below the tanker. As the vertical separation between the tanker and receiver increases, the amount of downwash encountered by the receiver decreases. Assuming no change in the pitch angle of the receiver, this reduced downwash results in an increased effective angle of attack, which increases the amount of lift generated by the receiver, resulting in a restorative lifting force. However, in the pitch axis, as the vertical separation between the tanker and receiver increases, and the amount of downwash encountered by the receiver decreases, and the increase in lift generated by the receiver

should result in a nose-down pitching moment, assuming the receiver has a C_m , α curve with a negative slope. In order to quantify the relationship between $\frac{\partial C_L}{\partial z}$ and $\frac{\partial C_m}{\partial z}$ in terms of positional stability, this paper introduces a new quantity called Positional Static Margin (SM_P). In flight dynamics, the static margin measures the distance from an aircraft's neutral point to its centre of gravity (CG). It can be measured directly as a percentage of the mean average chord by relating the $C_{m,\alpha}$ and $C_{L,\alpha}$ curves at a particular trim point as follows:

Static Margin =
$$-\frac{C_{m,\alpha}}{C_{L,\alpha}}$$
 (16)

The postional static margin uses an analogous form by relating the partial derivatives of C_L and C_m with respect to changes in position between tanker and receiver.

$$SM_P = \frac{\partial C_m / \partial z}{\partial C_L / \partial z} \tag{17}$$

While SM_P can also be a quantity of interest during PDR, it is not being examined in a PDR context in this work. The authors' previous work showed cross-coupling between the receiver's longitudinal and lateral/directional dynamic modes due to the receiver encountering asymmetric wake effects away from the tanker centreline [15]. By examining flying boom refueling, these asymmetric flight conditions can be minimized or eliminated, thus minimizing or eliminating cross-coupling, and making the longitudinal stability of the receiver far more relevant than the lateral/directional stability.

2.3 Longitudinal Axis Approximation and Frequency Analysis

In order to make use of this quantity for analysis of the AAR procedure, consider the longitudinal axis approximation given by Schmidt [19] in Equation 18, where the state variables are α and q, and the state matrix and input vector terms are defined in Table 1.

Table 1 – Dimensional Longitudinal stability derivatives [19]

Term	Description	Units
M_{lpha}	$\frac{QSc}{I_y}\frac{\partial C_m}{\partial \alpha}$	s^{-2}
$M_{\dot{lpha}}$	$\frac{QSc}{I_y}(\frac{c}{2V})\frac{\partial C_m}{\partial(\dot{\alpha}c/2V)}$	s^{-1}
M_q	$\frac{QSc}{I_y}(\frac{c}{2V})\frac{\partial C_m}{\partial (qc/2V)}$	s^{-1}
M_{δ}	$\frac{QSc}{I_y}\frac{\partial C_m}{\partial \delta}$	s^{-2}
Z_{α}	$\frac{QS}{m}(C_D - \frac{\partial C_L}{\partial \alpha})$	$\mathrm{m}{\cdot}\mathrm{s}^{-2}$
Z_{δ}	$\frac{QS}{m} \frac{\partial C_L}{\partial \delta}$	$\mathrm{m}{\cdot}\mathrm{s}^{-2}$

The effect of a change in displacement between the tanker and receiver can be expressed in terms of the change in pitching moment and lifting moment per unit change in displacement.

To perform a frequency analysis, we assume harmonic forcing with frequency ω based on small fluctuations in the position of the tanker and the receiver relative to each other. It is also assumed that there will be some phase shift $-\phi$ due to the time lag between the effect of the tanker on the main wing (primarily affecting the lifting coefficient) and the horizontal tail (primarily affecting the pitching moment). This time lag is assumed to be the distance between the wing and the horizontal tail divided by U_{∞} . For a negative value of SM_P , this essentially results in forcing of the pitching moment and lifting force that is 180 degrees out of phase, minus the phase shift due to time lag.

Wang et al. suggest that the flight path angle γ is a value of interest when evaluating handling qualities during AAR, and make recommendations for the frequency response of the flight path angle to the control stick position [20]. The flight path angle can be approximated as follows:

$$\frac{\gamma(s)}{q(s)} \approx \frac{L_{\alpha}}{s^2 + L_{\alpha}s} \tag{21}$$

where L_{α} is the derivative of the lift force with respect to angle of attack, normalized by the mass of the aircraft and U_{∞} .

$$L_{\alpha} = \left(\frac{\partial L}{\partial \alpha}/mU_{\infty}\right) \tag{22}$$

It can be assumed that the pilot of the receiver wishes to keep the flight path angle constant throughout the AAR procedure, and therefore will be making compensatory adjustments on the flight stick. The pilot behaviour and control stick position, c_p , here is approximated by a Tustin pilot model, which was initially proposed by Tustin in 1947. [21] In equation 23, the transfer function of the pilot's control behaviour, Y_P , is approximated by assuming some gain K_p , an anticipation time-lead constant T_L , and a time delay constant τ .

$$Y_P = \frac{c_p(s)}{e(s)} = \frac{K_p(1 + T_L s)e^{-\tau s}}{s}$$
 (23)

In the Tustin model, the gain K_p and time delay constant τ are representative of the pilot's observational and neuromuscular limitations, and the time-lead constant T_L is representative of the pilot's experience and ability to predict the behaviour of the aircraft. A schematic of the closed loop system can be seen in Figure 2.

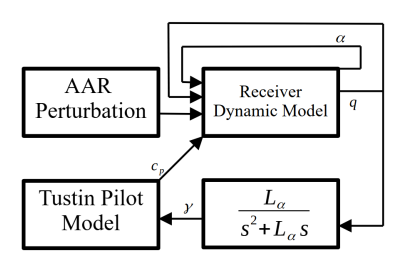


Figure 2 – MATLAB/Simulink model structure.

Based on this, the analysis proposed here is to examine $|\frac{\gamma}{\Delta z}(j\omega)|$, $\angle\frac{\gamma}{\Delta z}(j\omega)$, and $\angle\frac{\gamma}{\delta}(j\omega)$ based on the different values of $\partial C_m/\partial z$, $\partial C_L/\partial z$, and SM_P at different vertical separations for two tanker-receiver pairs: a KC-135 tanker with a C-5 receiver, and a KC-135 tanker with a C-17 receiver. Both receivers have a T-tail, meaning that SM_P in pitch at different elevations behind the tanker can differ significantly. Although the receiver geometries are similar, the C-5 is much longer than the C-17, meaning that it has a much smaller moment of inertia resulting in significantly different pitch axis dynamics. These

two similar aircraft have been selected for examination, because the C-17 has been reported to suffer from PIOs during AAR at high speeds before mitigation efforts [11, 22, 12], whereas the C-5 has not. Therefore, these two tanker-receiver pairs are excellent test cases which can demonstrate the analysis method's ability to predict different behaviours of two similar aircraft. The required longitudinal stability derivatives for the C-5 were taken from NASA Contractor Report CR-2144 [23], and the longitudinal stability derivatives for the C-17 were either approximated with using a VLM analysis or with the flight test data found in lloputaife [22], as necessary. A comparison of the model behaviour with flight test data found in lloputaife can be seen in Figure 3.

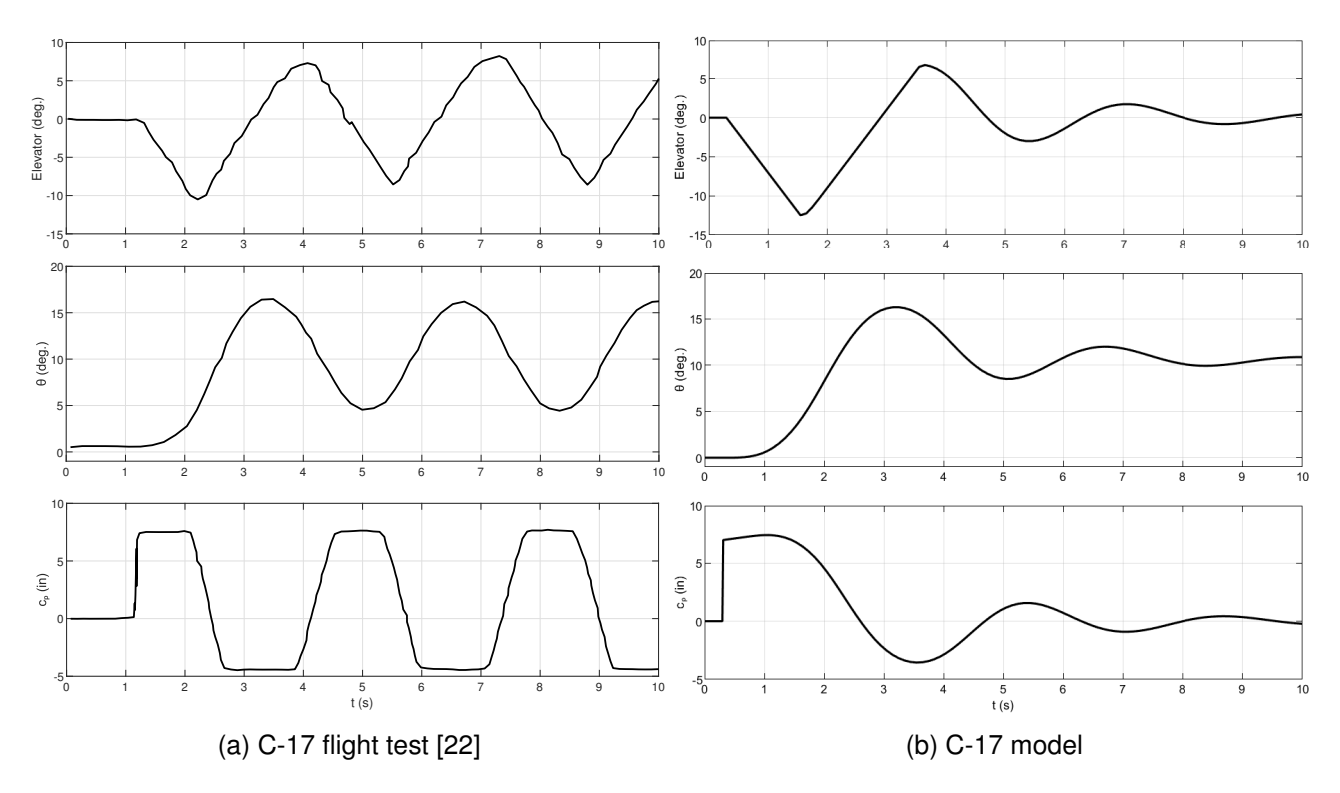


Figure 3 – Flight test and modeled results of a C-17 pitch step target test.

As detailed in Iloputaife, a step target analysis method was used to evaluate the entire control system. In the step target analysis, a desired pitch angle was set, in this case 10 degrees, and then the pilot is instructed to acquire the target as soon as possible without overshoot, and to stay on the target. The C-17 demonstrated PIO tendencies in this test before various changes were made to the control system. This version of the C-17 was used to derive values for the C-17 dynamic model and the Tustin pilot model. The resulting C-17 simulation controlled by the Tustin pilot model demonstrates similar rates and maxima in elevator deflection, pitch, and stick position when compared to the C-17 flight test. Additionally, the period of oscillation about the pitch target of 10 degrees is only slightly longer (0.5 seconds) than that of the flight test. The most notable difference is that the simulated C-17 model controlled by the Tustin pilot model does not go into limit cycle oscillations/PIOs. This is largely due to the nature of the Tustin pilot response, which is essentially a modified proportionalintegral controller. Such a controller will not provide the extremely rapid changes in control stick input seen in the flight test, thus giving the natural damping characteristics of the airplane time to damp out the oscillatory pitch behaviour. This makes the pilot model useful to establish a baseline "best-case" pilot response, which is consistent across all flight conditions and aircraft configurations. Undesirable behaviour demonstrated in this best-case scenario is unlikely to be improved by the input of a human pilot. The Tustin model parameters derived and used are given in Table 2.

Table 2 – Tustin Model Parameters

Aircraft	K_p	T_L	τ
C-17	0.2	10	0.3
C-5	0.14	10	0.3

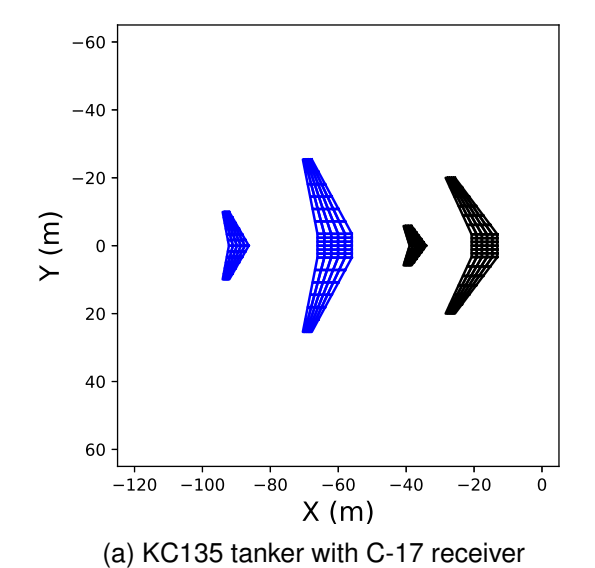
The discrepancy in K_p in the C-17 and C-5 pilot models is due to the difference in how the control inputs are defined. The C-17's pilot model is assumed to provide a stick displacement c_p , whereas the C-5's control system detailed in NASA Contractor Report CR-2144 requires a pilot stick force as input. [23] The value of K_p for the C-5 pilot model was chosen such that the maximum amount of stick force during an identical step target analysis did not exceed 75 lbs. Although this may seem large, the C-5's stick stiffness at nominal refueling conditions is 28 lbs/in., so a stick force of 75 lbs. represents a stick travel of 2.67 in., which is one third of that of the C-17.

3 Results and Discussion

Table 3 – Refueling Conditions

Parameter	Value	Units
Airspeeds	144.2, 170.6, 212.5	m/s
Altitude	20,000	ft.
$ ho_{\scriptscriptstyle \infty}$	0.653	kg/m ³
a	316	m/s
M_{∞}	0.46, 0.54, 0.67	-

The three flight conditions examined can be seen in Table 3 and a typical alignment of the aircraft during AAR can be seen in Figure 4. Both receivers are depicted at the approximate contact point. The three flight conditions chosen correspond to a low speed, nominal, and high speed refueling process at 20,000 ft. Notably, M=0.67 was the point at which the C-17 began to exhibit PIO tendencies during refueling [11].



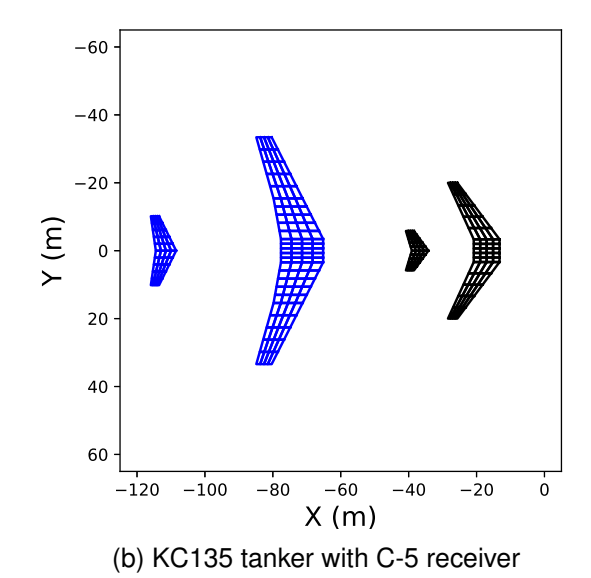


Figure 4 – Typical alignment of tanker and receiver lifting surfaces during AAR.

A comparison of the longitudinal positional stability at various vertical separations can be seen in Figure 5. The vertical separation between the tanker and receiver is measured from the level of the wing planform of the tanker at Y = 0 to the level of the wing planform of the receiver at Y = 0.

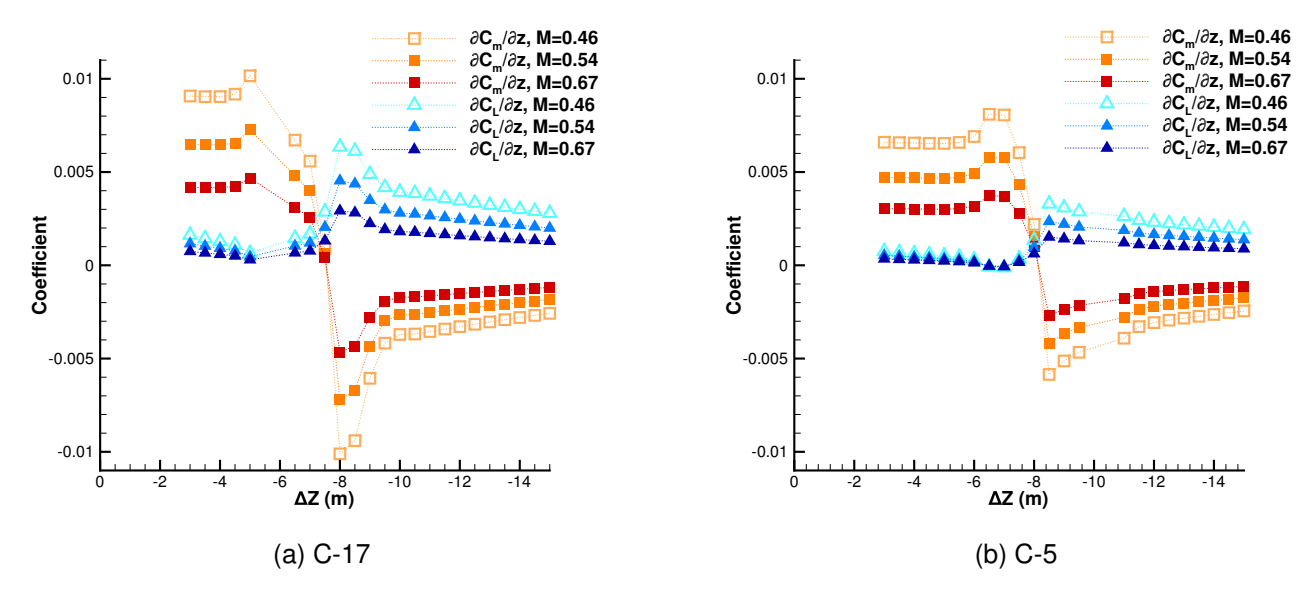


Figure 5 – Comparison of longitudinal positional stability of a C-17 and C-5 receiver during aerial refueling quantities at various vertical separations.

The C-17 and C-5 both demonstrate similar positional stability traits, showing a positive value for $\frac{\partial C_m}{\partial z}$ and a smaller value of $\frac{\partial C_L}{\partial z}$ at smaller vertical separations up until some crossover point. This is due to the height difference between the wing and tail planforms. At small vertical displacements, as the receiver moves downwards, the main wings encounter less downwash leading to an increased lift force. In contrast, the tail encounters more downwash, which increases the nose-up pitching moment on the entire aircraft. This persists as the vertical displacement increases until the the tail passes through the region of maximum downwash. After this point, the downwash decreases with increased vertical displacement, increasing the lift generated by the tail, and resulting in a nose-down pitching moment. For the C-17, the crossover point occurs around $\Delta z = 7.5$ m and for the C-5, this crossover point occurs around $\Delta z = 8$ m. This crossover point is at a vertical separation at which the level of each receiver's tail is between the level of the tanker's horizontal stabilizer and wing. After this crossover point, $\frac{\partial C_m}{\partial z}$ becomes negative, and $\frac{\partial C_L}{\partial z}$ becomes more positive, with the C-17 exhibiting greater sensitivity to small changes in relative position, with the region of greatest sensitivity corresponding to the level of the T-tail being just below the level of the receiver wings, and therefore in the region of maximum downwash. The flying boom of the KC-135 extending between 6.5m and 9m vertically, and therefore this is the range of vertical separations that will be considered in the following figures. It should also be noted that the KC-135 typically prefers to refuel at as large a vertical separation as possible, so as to limit the bow wave effect from the much large aircraft being refueled.

Figure 6 shows a typical Bode plot generated using the model diagrammed in Figure 2, assuming M=0.54, and initial vertical separation is 8.0 m. The input is assumed to be some change in vertical separation between tanker and receiver, and the outputs examined here are the response of the flight path angle γ and the response of the pilot trying to keep the flight path angle γ constant. The pilot response is represented by the stick position c_p measured in cm.

At the vertical separation of 8.0 m, $\frac{\partial C_m}{\partial z}$ is negative, indicating that an increase in separation between the aircraft will result in a nose down pitching moment. This is represented in the Bode plot by the response of γ and c_p being close to 180 degrees out of phase with the perturbation at low frequencies. As the frequency increases, the phase difference between the perturbation and the aircraft and pilot response goes towards zero degrees at some crossover frequency, f_c , where $\angle \frac{\gamma}{\Delta z}(f_c) = 0$. This crossover frequency is analogous to the minimum possible frequency of the aircraft and pilot response that can allow the receiver to control its flight path and relative position behind the tanker assuming pilot inputs of the magnitude given by $\frac{c_p}{\Delta z}$. The crossover frequency of γ shown in Figure

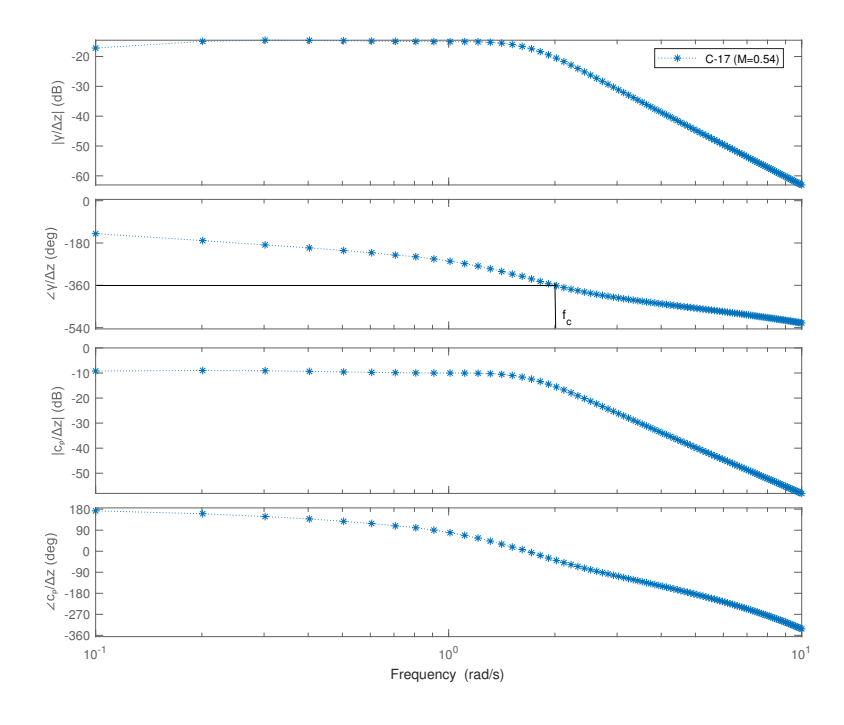


Figure 6 – Bode plot of a C-17 receiver and pilot response to a perturbation caused by a change in vertical separation between tanker and receiver. M_{∞} = 0.54, Δz = 8.0m.

6 is 2 rad/s. Therefore, it is predicted that maneuvers during the AAR procedure must be performed by the pilot at a frequency no less than 2 rad/s, or the flight path response and relative separation between tanker and receiver will fall out of phase. An example of the aircraft and pilot response at this crossover frequency of 2 rad/s can be seen in Figure 7.

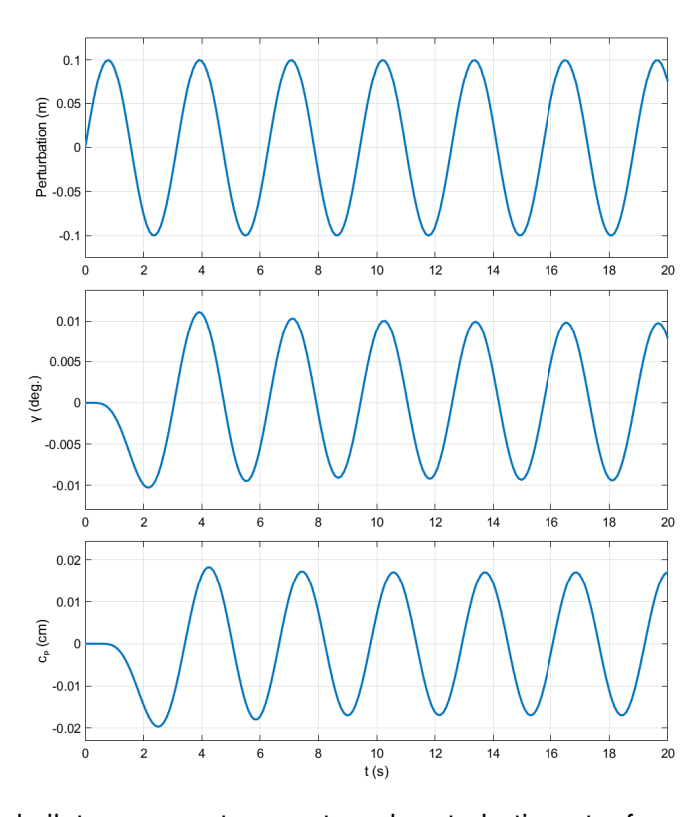


Figure 7 – Aircraft and pilot response to an external perturbation at a frequency of 2.0 rad/s, and initial vertical separation of 8.0 m.

Figure 7 shows the aircraft flight path angle response in phase with the perturbation, with the pilot response slightly lagging in phase behind the flight path angle response. This phase lag is largely a function of the Tustin model time delay constant, τ , and can be artificially removed by arbitrarily setting $\tau=0$. The aircraft response to external perturbation at $\Delta z=8.0$ m can be contrasted to the Bode plot of the same flight condition, where $\Delta z=7.0$ m, seen in Figure 8.

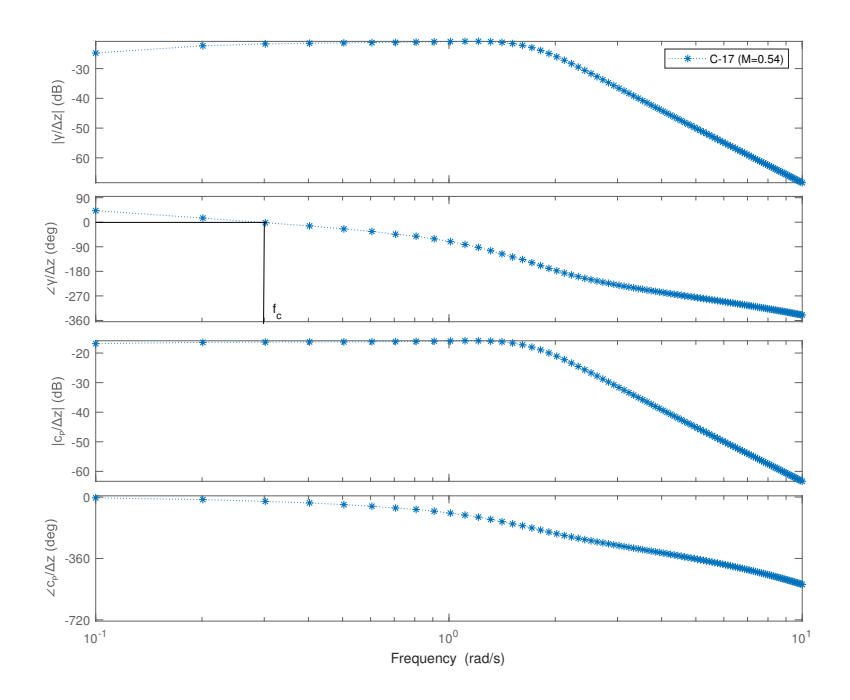


Figure 8 – Bode plot of a C-17 receiver and pilot response to a perturbation caused by a change in vertical separation between tanker and receiver. M_{∞} = 0.54, Δz = 7.0m.

As can be seen in Figure 5, the a vertical separation of 7.0 m, $\frac{\partial C_m}{\partial z}$ is positive, implying that an increase in vertical separation between tanker and receiver will result in a pitch up moment, and vice versa. This is reflected in Figure 8, as it can be seen that the crossover frequency is very low. This implies that minimum frequency of control inputs that will allow the pilot to control the receiver's flight path this vertical separation is very slow, as the receiver is stable with respect to position relative to the tanker. The aircraft and pilot response at this very low crossover frequency can be seen in Figure 9.

Given the very slow external forcing and aircraft response, it is easy to see that a pilot reaction and response that is given at a higher frequency than that of the perturbation will be capable of keeping the change in γ throughout the oscillation close to 0. Likewise, it can be seen in Figure 7 that a slower pilot input will result in the aircraft falling out of phase with the perturbation. This is why the crossover frequency, f_c , was selected as the frequency of interest for the analysis. A summary of the crossover frequencies for both the C-17 and C-5 receivers at vertical separations between 6.5 m and 9.0 m can be seen in Figure 10.

In general, the crossover frequency is a function of the positional stability at each vertical separation, although the exact crossover frequency is still dependent on the flight condition and aircraft dynamic characteristics. The magnitude of the pilot response is also examined at the crossover frequencies, in addition to the phase difference between the pilot inputs and aircraft response. This can be seen in Figure 11.

The pilot compensation phase shown in Figure 11 is the phase difference between the pilot and the response of the receiver flight path angle at the crossover frequency. This is a function of the time delay used in the Tustin pilot model. The resonance of the pilot input of the C-5 decreases with in-

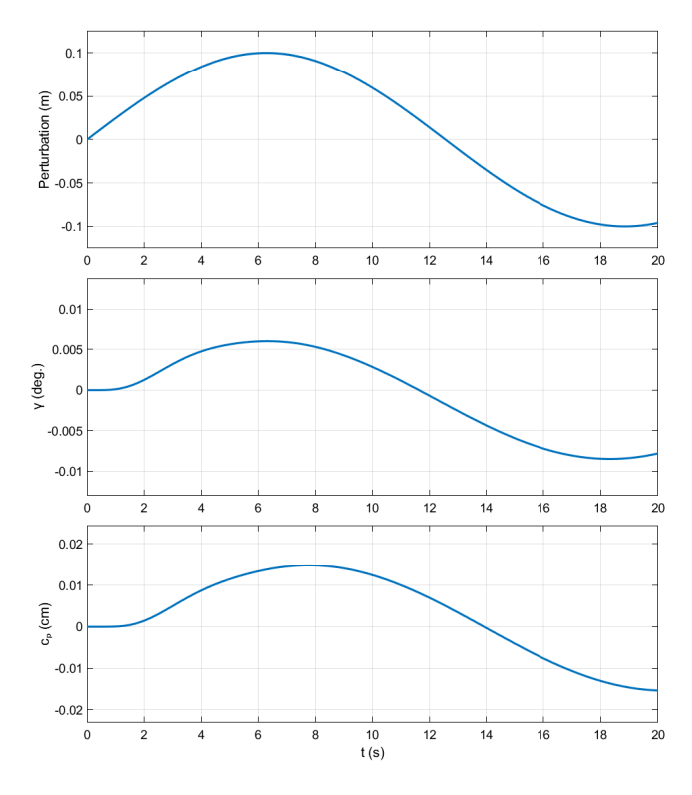


Figure 9 – Aircraft and pilot response to an external perturbation at a frequency of 0.16 rad/s, and initial vertical separation of 7.0 m.

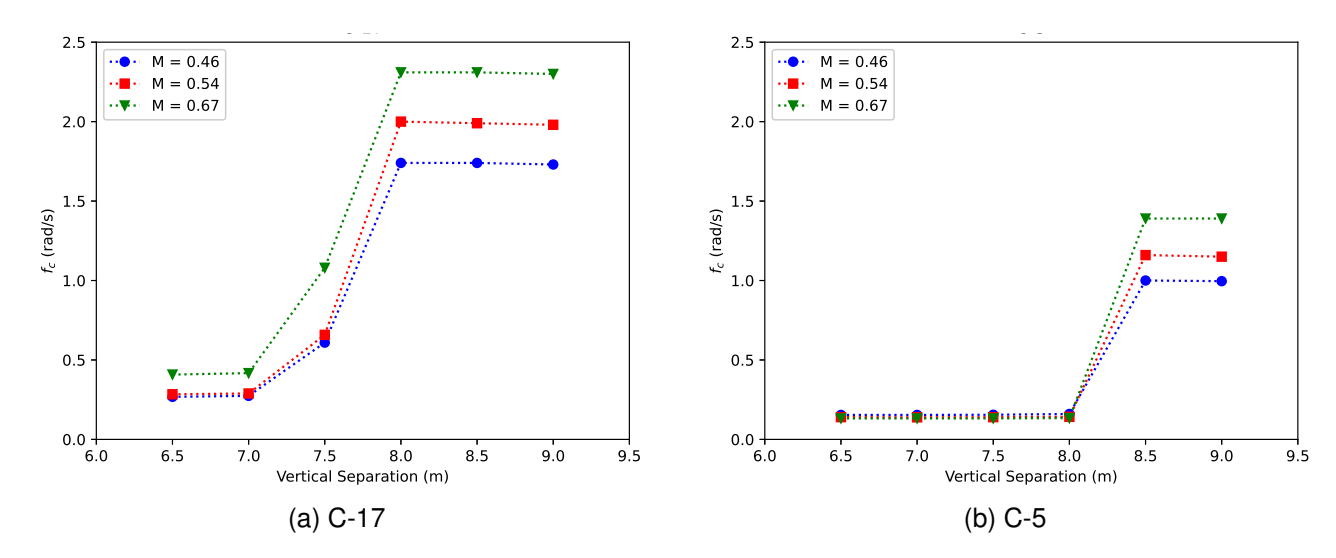


Figure 10 – Crossover frequencies for the C-17 and C-5 at various flight conditions and separations between tanker and receiver.

creased vertical separation, whereas the pilot input resonance of of the C-17 drastically decreases at $\Delta z = 7.5$ m. This can be partially predicted using the SM_P values of both aircraft. Figure 12 compares the SM_P of both receivers at vertical separations from 6.5 m to 9 m in terms of the log of the absolute value of SM_P . At all examined airspeeds, the magnitude of both the $\frac{\partial C_L}{\partial z}$ and $\frac{\partial C_m}{\partial z}$ derivatives is reduced as airspeed increases, but interestingly, SM_P remains unchanged, suggesting that the relationship between the positional stability quantities is a fundamental quality of the tanker-receiver pair, rather than a function of flight conditions.

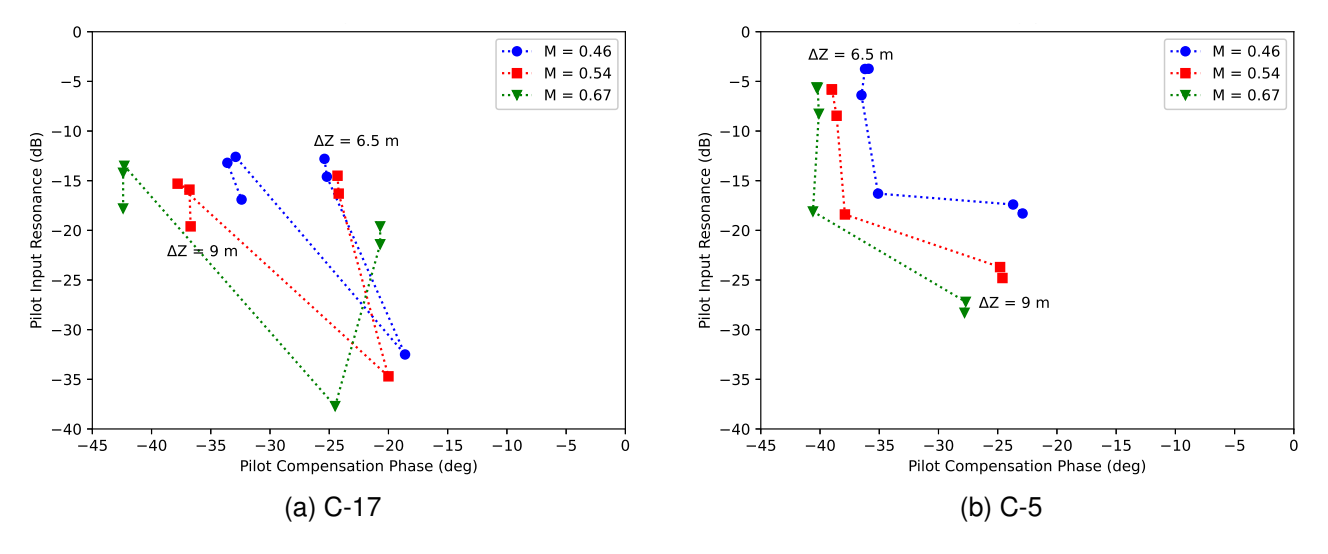


Figure 11 – Phase difference between pilot input and aircraft response and pilot input resonance at crossover frequency at various flight conditions and separations between tanker and receiver.

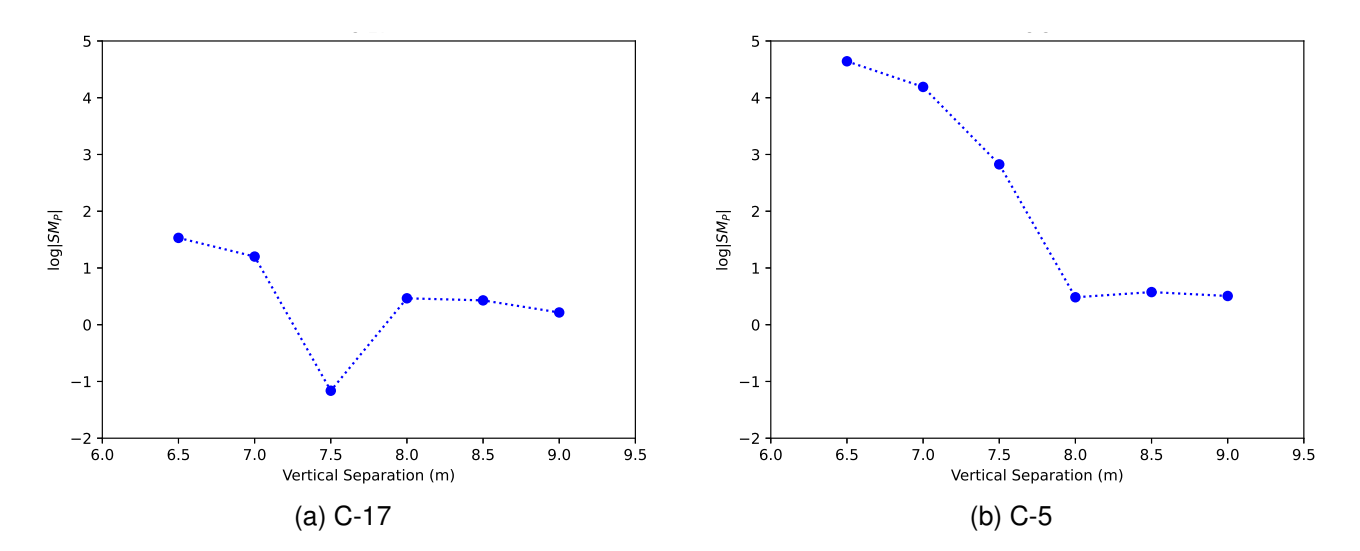


Figure $12 - \log |SM_P|$ at various vertical separations between tanker and receiver.

 SM_P is much larger for the C-5 than for the C-17 at the smaller vertical separations, owing to the extremely small values of $\frac{\partial C_L}{\partial z}$ up until the crossover point. The C-17 exhibits one area at $\Delta z=7.5$ m where $\frac{\partial C_L}{\partial z}$ is much larger than $\frac{\partial C_M}{\partial z}$, resulting in a comparatively small value of SM_P . In general, it can be seen that the magnitude of the pilot responses in Figure 11 is related to $\log |SM_P|$, although the precise relationship between to the magnitude of the pilot input is dependent on factors, such as gains within the closed loop system. Based on this, it can be assumed that the C-5 also has a vertical separation between $\Delta z=8.0$ m and $\Delta z=8.5$ m at which the value of $\log |SM_P|$ is very small, due to the neutral positional stability in the pitch axis. This "Goldilocks Zone" of small $\log |SM_P|$ exists roughly at vertical separations where the horizontal tail plane is at a height between the tail plane and wing plane of the tanker. However, due to the larger tail of the C-5, this occurs at a larger vertical separation that that of the C-17, which would be considered preferable for the KC-135 tanker.

Based on the crossover frequency and the phase difference between the pilot and the aircraft response at the crossover frequency, ϕ_{C_p} , we define a time delay margin as follows:

$$\tau_{d_{\text{margin}}} = \frac{\frac{\pi}{2} + \phi_{c_p}}{f_c} \tag{24}$$

The time delay margin is a measure of how much total system equivalent time delay can be allowed in the higher order system before the pilot and aircraft response become 90 degrees out of phase at

the crossover frequency, assuming a pilot reaction time of 0.3s. A plot of the pilot input resonance as a function of the time delay margin can be seen in Figure 13.

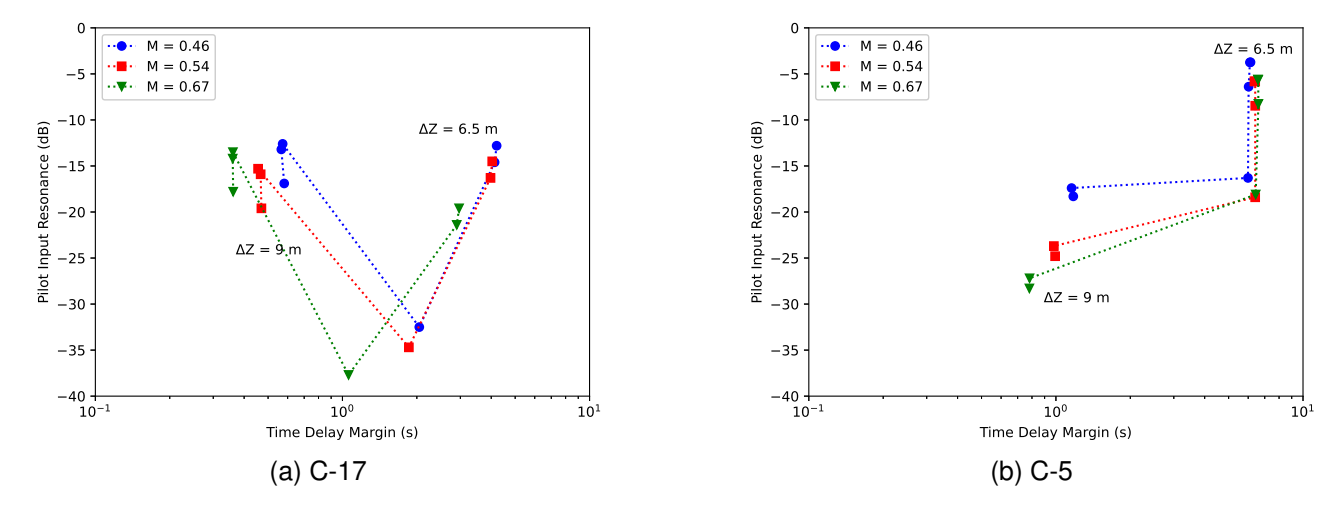


Figure 13 – Time delay margin and pilot input resonance at various flight conditions and vertical separations.

Figure 13 shows that at small vertical separations, although the pilot input resonance is comparatively high, the low crossover frequency allows the pilot ample time to correct any effect of disturbances. As the vertical separation increase, this time delay margin reduces down to the order of 1 second, but the pilot input resonance is reduced. This indicates favourable handling qualities for the pilot, where changes to pilot input based on disturbances from the tanker can be small and slow. In contrast, the time delay margin of the C-17 at vertical separations of 8.0 m to 9.0 m runs from 560 ms at low speeds to 360 ms at the high speed flight condition, and the pilot input resonance is also up to 10 dB higher than that of the C-5. This combination of higher pilot input resonance and the requirement of shorter pilot input timescales leading to a smaller time delay margin are likely to be factors which are indicative of the potential for PIOs during the AAR task. To demonstrate this, a time trace of the aircraft and pilot response to a perturbation at $M_{\infty} = 0.672$ and $\Delta z = 9.0$ m where the pilot response delay, τ , has been increased to 0.75s, can be seen in Figure 14.

Given that the initial pilot reaction delay was 0.3 seconds, and the time delay margin at this flight condition was 0.38 s, the time delay margin in this scenario is effectively negative. It can be seen that the aircraft and pilot response grows over a period of 60 seconds, indicating that the aircraft is extremely likely to enter a PIO regime. This effect could be further exacerbated by making small increases to the pilot or control system gains. The relevance of pilot input resonance and time delay margin is further supported by the documentation of the efforts which were undertaken to mitigate the PIOs of the C-17, which involved pitch stick shaping, effectively reducing pilot input gain and resonance [11], and reducing the time delay in the higher order system by 150 ms with a combination of filter changes [22, 12], and the addition of stick force command path lead in the pitch axis [12].

This methodology has utility in tanker-receiver compatibility analysis in terms of making reasonable predictions about the nature of the pilot and aircraft response during high gain tracking tasks such as AAR, although higher order system effects are neglected. It could also be used early in the design process for predicting AAR performance before all aspects of the higher-order control system are known. Additionally, its use of the Tustin model removes the necessity of performing simulator tests immediately, and the general methodology can be adapted for use with remotely piloted flight control systems, as the time delay could be tuned to be better representative of the remote pilot system delays. Future work and pilot testing could place reasonable bounds on the metrics discussed to allow for prediction of AAR-specific handling qualities.

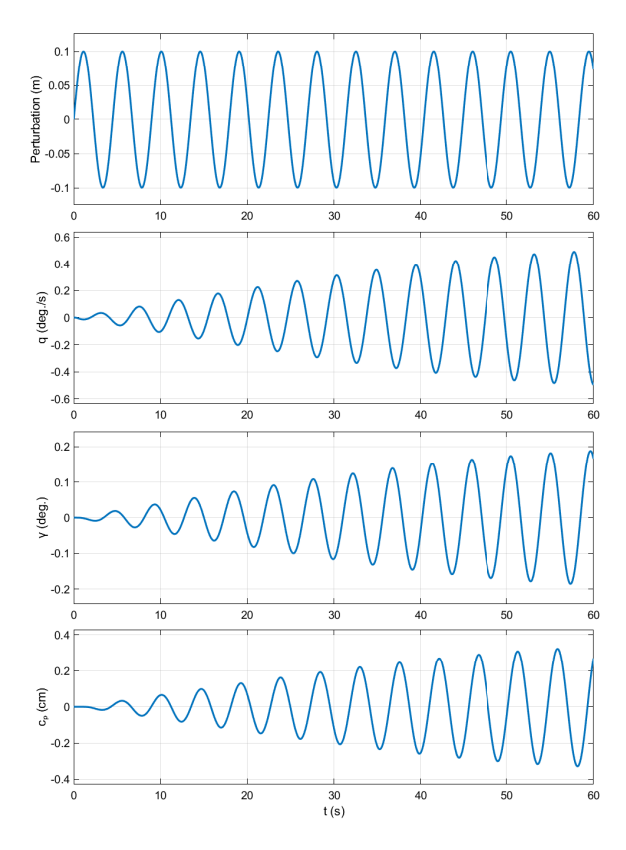


Figure 14 – Aircraft and pilot response to a perturbation of 1 rad/s at M_{∞} = 0.672 and Δz = 9.0 m when response delay is increased to τ = 0.75s.

4 Conclusion

This paper used a combination of computational methods to examine aircraft and pilot response of the C-17 and C-5 during the flying boom AAR procedure with a KC-135 tanker at three different flight conditions. New metrics for evaluating receiver performance during the AAR task were introduced by examining the positional stability characteristics of the tanker/receiver pair, the resonance of the pilot inputs, and the phase difference between changes in the vertical separation and the response of the flight path angle at different perturbation frequencies. Results showed that pilot inputs to perturbations were smaller for the C-5 compared to the C-17 as the frequency of interest, the crossover frequency, was increased. In addition, flight path control of the C-17 was shown to necessitate higher frequency and higher amplitude pilot inputs, leading to the potential for PIOs at high speeds assuming equivalent system time delays on the order of 100 ms. The utility of this analysis framework is supported by the history of PIOs demonstrated by the C-17 during AAR, which necessitated changes to control system gains and equivalent system time delays to ameliorate. In the future, it may be used in the design process to create guidelines for higher-order control system delays, or creating gain scheduling guidelines specific to the AAR task.

5 Acknowledgments

The authors wish to acknowledge and thank the Directorate of Technical Airworthiness and Engineering Support (DTAES) at Canada's Department of National Defence (DND) for supporting this research (Grant #18485SK101-07).

6 Contact Author Email Address

mailto: luke.peristy at rmc.ca mailto: ruben.perez at rmc.ca

7 Copyright Statement

The authors confirm that they, and/or their company or organization, hold copyright on all of the original material included in this paper. The authors also confirm that they have obtained permission, from the copyright holder

of any third party material included in this paper, to publish it as part of their paper. The authors confirm that they give permission, or have obtained permission from the copyright holder of this paper, for the publication and distribution of this paper as part of the ICAS proceedings or as individual off-prints from the proceedings.

References

- [1] Toydas, M., Fuel savings opportunities from air refueling, Master's thesis, Air Force Institute of Technology, 2010.
- [2] Nangia, R., "Operations and aircraft design towards greener civil aviation using air-to-air refuelling," *Aeronautical Journal*, Vol. 110, No. 1113, 2006, pp. 705–721.
- [3] Spencer, R., "Predicting the certification basis for airliner air-to-air refuelling," *The Aeronautical Journal*, Vol. 119, No. 1220, 2015, pp. 1175–1192.
- [4] Bloy, A., Lamont, P., Abu-Assaf, H., and Ali, K., "The lateral dynamic stability and control of a large receiver aircraft during air-to-air refuelling," *Aeronautical Journal*, Vol. 90, 1986, pp. 237–243.
- [5] Bloy, A., Ali, K., and Trochalidis, V., "The longitudinal dynamic stability and control of a large receiver aircraft during air-to-air refueling," *Aeronautical Journal*, Vol. 91, No. 902, 1987, pp. 64–71.
- [6] Bloy, A. and Trochalidis, V., "The performance and longitudinal stability and control of large receiver aircraft during air to air refuelling," *Aeronautical Journal*, Vol. 93, No. 930, 1989, pp. 367–378.
- [7] Blake, W., "An Aerodynamic Model for Simulation of Close Formation Flight," *AIAA Modeling and Simulation Technologies Conference and Exhibit*, No. AIAA 2000-4304, Air Force Research Laboratory, AIAA, Denver, CO, August 2000.
- [8] Blake, W. and Gingras, D., "Comparison of Predicted and Measured Formation Flight Interference Effects," *Journal of Aircraft*, Vol. 41, No. 2, March–April 2004, pp. pp. 201–207.
- [9] Dogan, A. and Blake, W., "Modeling of bow wave effect in aerial refueling," *AIAA Atmospheric Flight Mechanics Conference*, 2010, p. 7926.
- [10] Okolo, W., Dogan, A., and Blake, W., "Effect of trail aircraft trim on optimum location in formation flight," *Journal of Aircraft*, 2015.
- [11] Iloputaife, O., Svoboda, G., and Bailey, T., "Handling qualities design of the C-17A for receiver-refueling," *Guidance, Navigation, and Control Conference*, 1996, p. 3746.
- [12] Weltz, G. I., Barajas, M. G., and Shweyk, K. M., "Improvements in Aerial Refueling Flight Control System for a Large Receiver Aircraft," *AIAA Scitech 2021 Forum*, 2021, p. 0716.
- [13] Mitchell, D. G. and Klyde, D. H., "Identifying a pilot-induced oscillation signature: New techniques applied to old problems," *Journal of Guidance, Control, and Dynamics*, Vol. 31, No. 1, 2008, pp. 215–224.
- [14] Yin, H., Wang, L., Yue, T., and Liu, H., "Pilot-Induced Oscillation Analysis for Receiver in Flying-Boom Aerial Refueling via Mission-Oriented Evaluation," 2019 IEEE 10th International Conference on Mechanical and Aerospace Engineering (ICMAE), IEEE, 2019, pp. 47–51.
- [15] Peristy, L. and Perez, R., "Trim Strategies and Dynamic Cross-Coupling During Aerial Refueling," *CEAS Aeronautical Journal*, Vol. 14, 2023, pp. 817–834.
- [16] Katz, J. and Plotkin, A., Low-speed aerodynamics, Vol. 13, Cambridge University Press, 2001.
- [17] Dogan, A., Blake, W., and Haag, C., "Bow Wave Effect in Aerial Refueling: Computational Analysis and Modeling," *Journal of Aircraft*, Vol. 50, No. 6, 2013, pp. 1856–1868.
- [18] Jackson, D., Tyler, C., and Blake, W., "Computational analysis of air-to-air refueling," *25th AIAA Applied Aerodynamics Conference*, 2007, p. 4289.
- [19] Schmidt, L. V., *Introduction to aircraft flight dynamics*, American Institute of Aeronautics and Astronautics, 1998.
- [20] Wang, L., Yin, H., Guo, Y., Yue, T., and Jia, X., "Closed-loop motion characteristic requirements of receiver aircraft for probe and drogue aerial refueling," *Aerospace Science and Technology*, Vol. 93, 2019, pp. 105293.
- [21] Tustin, A., "The nature of the operator's response in manual control, and its implications for controller design," *Journal of the Institution of Electrical Engineers-Part IIA: Automatic Regulators and Servo Mechanisms*, Vol. 94, No. 2, 1947, pp. 190–206.
- [22] Iloputaife, O., "Minimizing pilot-induced-oscillation susceptibility during C-17 development," *22nd Atmospheric Flight Mechanics Conference*, 1997, p. 3497.
- [23] Heffley, R. K. and Jewell, W. F., "Aircraft handling qualities data," Tech. rep., NASA, 1972.